Optimal transient growth and very large-scale structures in turbulent boundary layers

Carlo Cossu, Gregory Pujals, Sebastien Depardon

Optimal transient growth and very large–scale structures in turbulent boundary layers

CARLO COSSU[1]†, GREGORY PUJALS[1,2] AND SEBASTIEN DEPARDON[2]

[1]LadHyX, CNRS-École Polytechnique, F-91128 Palaiseau, France

[2]PSA Peugeot Citroën, Centre Technique de Velizy, 2 Route de Gisy, 78943 Vélizy-Villacoublay Cedex, France

The optimal energy growth of perturbations sustained by a zero pressure gradient turbulent boundary is computed using the eddy viscosity associated with the turbulent mean flow. It is found that even if all the considered turbulent mean profiles are linearly stable, they support transient energy growths. The most amplified perturbations are streamwise uniform and correspond to streamwise streaks originated by streamwise vortices. For sufficiently large Reynolds numbers two distinct peaks of the optimal growth exist, respectively scaling in inner and outer units. The optimal structures associated with the peak scaling in inner units correspond well with the most probable streaks and vortices observed in the buffer layer, and their moderate energy growth is independent of the Reynolds number. The energy growth associated with the peak scaling in outer units is larger than that of the inner peak and scales linearly with an effective turbulent Reynolds number formed with the maximum eddy viscosity and a modified Rotta–Clauser length based on the momentum thickness. The corresponding optimal perturbations consist of very large–scale structures with a spanwise wavelength of the order of 8δ. The associated optimal streaks scale in outer variables in the outer region and in wall units in the inner region of the boundary layer, in which they are proportional to the mean flow velocity. These outer streaks protrude far into the near wall region, having still 50 % of their maximum amplitude at $y^+ = 20$. The amplification of very large–scale structures appears to be a robust feature of the turbulent boundary layer: optimal perturbations with spanwise wavelengths ranging from 4δ to 15δ can all reach 80 % of the overall optimal peak growth.

1. Introduction

The presence of persistent streaky structures is a well-established robust feature of turbulent shear flows (Kline *et al.* 1967). A large amount of research has been dedicated to the understanding of the mechanisms by which streaks are generated and of their relevance to the turbulent dynamics. In the near wall region of the boundary layer these streaks, with characteristic mean spacing of about 100 wall units, are thought to play an essential role in a turbulent self-sustained mechanism (Jiménez & Moin 1991; Hamilton, Kim & Waleffe 1995; Waleffe 1995). The 'lift-up' effect by which low-energy streamwise vortices can induce large-energy streaks

† Email address for correspondence: Carlo.Cossu@ladhyx.polytechnique.fr

(Moffatt 1967; Ellingsen & Palm 1975; Landahl 1980) is an important process embedded in this self-sustained mechanism. The same effect, leading to unstable large-amplitude streaks, is also thought to play a crucial role in the subcritical transition to turbulence in linearly stable shear flows (e.g. Kreiss, Lundbladh & Henningson 1994; Reddy *et al.* 1998). In the latter context it has been recognized that the energy amplification of the streaks, which is transient in time and proportional to the square of the Reynolds number (Gustavsson 1991), is related to the non-normal nature of the linearized Navier–Stokes operator and can lead to very large energy growths if optimized (Butler & Farrell 1992; Trefethen *et al.* 1993; Farrell & Ioannou 1996; Schmid & Henningson 2001). Recent studies have also demonstrated that the well-controlled optimal transient growth of artificially forced streaks can be efficiently used to manipulate at leading order laminar shear flows. Such a paradigm has been successfully applied to stabilize Tollmien–Schlichting waves in a laminar boundary layer (Cossu & Brandt 2002; Fransson *et al.* 2005) and effectively delay the transition to turbulence (Fransson *et al.* 2006). In these investigations, roughness elements were used to create nearly optimal vortices in the upstream part of the boundary layer that induced well-controlled streamwise streaks downstream. A still-not-addressed extension of such a kind of approach would consist in the manipulation of turbulent boundary layers with optimal vortices and streaks, the first step in this direction being to compute the optimal perturbations of the turbulent boundary layer.

If the optimal energy growth and the corresponding optimal perturbations have been computed for virtually all the canonical wall-bounded laminar shear flows, only few studies have considered turbulent flows. Linear stability analyses of turbulent mean basic flows by Malkus (1956), Reynolds & Tiederman (1967) and Reynolds & Hussain (1972) essentially reveal that these flows are linearly stable. Only recently, the optimal-perturbation energy growth of turbulent mean flows has been investigated looking for a relation between turbulent coherent structures and linear optimals (Butler & Farrell 1993; Farrell & Ioannou 1993, 1998). Butler & Farrell (1993) considered the optimal perturbations of a turbulent channel flow, using the Reynolds & Tiederman (1967) turbulent mean profile based on the eddy viscosity model of Cess (1958), but they used the molecular viscosity in the equations for the perturbations. They found that perturbations leading to maximum growth are streamwise uniform and spanwise periodic with wavelength near $3h$, where h is the channel half-width, which is almost the same value selected in the laminar case. By constraining the optimization to times of the order of the eddy turnover time they were able to find optimals with the typical 100 wall units spacing characteristic of the near wall region streaks. del Álamo & Jiménez (2006) repeated the analysis, using in the linear operator the eddy viscosity $\nu_T(y)$ associated with the turbulent mean flow in the spirit of the modal linear investigations of Reynolds & Hussain (1972). Without any further restriction on the optimization times they found two peaks for the optimal growth. The main peak scales on external units with an optimal spanwise wavelength $\lambda_z \sim 3h$, while the secondary peak, which scales in inner (wall) units, is found at $\lambda^+ = 100$ and is associated with typical near wall streaks. To explain the formation of secondary vortices in a turbulent square duct Bottaro, Souied & Galletti (2006) have computed the linear optimals, using a mixing length model for the eddy viscosity.

The optimal perturbation energy growth has not yet been computed for turbulent boundary layers despite their great practical and theoretical relevance. For such type of flow some questions arise: Do two different optimal peaks with distinct scalings also appear in this case as expected? Which is the relevant external boundary layer length on which the optimal vortices and streaks scale? What are the values of the

optimal spanwise wavelengths? In the laminar case the optimal energy growth is proportional to the square of the Reynolds number. In the turbulent channel flow case the maximum growth of near wall structures does not seem to depend on the Reynolds number while the maximum growth of the large-scale structures does, but no characteristic scaling was found in that case. Another question therefore is on which quantity does the maximum energy growth of the large-scale structures scale? Answers to these questions, in addition to their relevance for the analysis of natural large-scale structures in turbulent boundary layers, will probably also be useful in the light of the many previous studies related to the manipulation of turbulent boundary layers with streamwise vortices by either riblets or bio-inspired rough walls scaling in inner units and vortex generators scaling in outer units. In most of these investigations, the particular choice of the actuator size and spacing have been inspired by bio-mimetic or semi-empirical considerations and not optimal energy growth considerations.

The scope of the present study is therefore to answer some of the questions proposed above by computing the optimal energy growth and the associated optimal perturbations supported by turbulent zero pressure gradient boundary layers. In §2 we briefly introduce the equations defining the turbulent mean flow, the procedure by which the associated turbulent shear stress and eddy viscosity are computed and the linearized equations for the perturbations, and we summarize how optimal perturbations and growths are computed. The optimal growths and perturbations computed for the selected mean flow profiles and their dependence on the streamwise and spanwise wavenumbers as well as on the Reynolds number are presented in §3. A summary of our findings and a discussion of their relation with existing studies and of their implications are provided in §4.

2. Background

2.1. *Mean flow and the associated eddy viscosity*

The boundary layer mean flow $U(x, y)$, $V(x, y)$ in the absence of pressure gradient in the streamwise direction x satisfies the standard mean mass and momentum conservation equations (see, e.g. Schlichting 1979):

$$\frac{\partial U}{\partial x} + \frac{\partial V}{\partial y} = 0, \tag{2.1}$$

$$U\frac{\partial U}{\partial x} + V\frac{\partial U}{\partial y} = \frac{1}{\rho}\frac{\partial \tau}{\partial y}, \tag{2.2}$$

where $\tau/\rho = \nu(\partial U/\partial y) - \langle u'v'\rangle/\rho$ is the sum of the molecular and the Reynolds shear stress. We denote by x, y and z respectively the streamwise, the wall normal and the spanwise coordinates. At sufficiently large Reynolds numbers, the boundary layer mean flow data can be conveniently fitted with uniformly valid asymptotic expansions, even if the validity of such an approach is a recurrent subject of debate. Here, we use a convenient self-consistent expression, recently proposed by Monkewitz, Chauhan & Nagib (2007), which very well fits the experimental data of Österlund (1999) and Nagib, Christophorou & Monkewitz (2004), among others, for a wide range of Reynolds numbers:

$$U = u_\tau \left[U_i^+(y^+) - U_{log}^+(y^+) + U_e^+(Re_{\delta_*}) - U_w^+(\eta) \right], \tag{2.3}$$

where $u_\tau = (\nu dU/dy|_{wall})^{1/2}$ is the wall friction velocity; $y^+ = yu_\tau/\nu$ is the wall normal coordinate scaled in inner units; $U_e{}^+ = U_e/u_\tau$ is the free-stream velocity U_e scaled with u_τ; $Re_{\delta_*} = U_e\delta_*/\nu$ is the Reynolds number scaled on the displacement thickness δ_*; and $\eta = y/\Delta$ is the wall normal coordinate scaled with the Rotta–Clauser outer length scale $\Delta = \delta_* U_e{}^+$. The inner and the outer coordinates are related by $y^+ = Re_{\delta_*}\eta$. The explicit expressions for the inner layer velocity function $U_i^+(y^+)$, the log layer velocity $U_{log}^+(y^+)$, the wake function $U_w^+(\eta)$ and $U_e{}^+$ are given in Appendix A. The quantitative results presented in the following of course apply only where (2.3) is a good fit to the data; however the procedure is general and could be applied to other expressions assumed for U.

The shear stress associated with the mean flow U can be retrieved by integrating (2.2) in the wall normal direction:

$$\frac{\tau(y)}{\rho} = u_\tau^2 + \int_0^y \left(U\frac{\partial U}{\partial x} + V\frac{\partial U}{\partial y} \right) dy, \qquad (2.4)$$

where the normal velocity component V can be computed with an integration of the continuity equation $V = -\int_0^y (\partial U/\partial x)\,dy$. An explicit expression for $\partial U/\partial x$ can be obtained deriving (2.3) with respect to x which, using the chain rule and (A 3) and after some manipulation, gives

$$\frac{1}{u_\tau}\frac{\partial U}{\partial x} = \frac{1}{u_\tau}\frac{du_\tau}{dx}\left[\frac{U}{u_\tau} + y^+\frac{\partial U_i^+}{\partial y^+} \right] + \frac{1}{\Delta}\frac{d\Delta}{dx}\left[\eta\frac{\partial U_w^+}{\partial \eta} + \frac{1}{\kappa} \right], \qquad (2.5)$$

where κ is the von Kármán 'coefficient'. Deriving with respect to x the explicit expression of $U_e{}^+$ (A 3), and recalling that in the zero pressure gradient boundary layer $dU_e/dx = 0$, it is found that

$$\frac{1}{\Delta}\frac{d\Delta}{dx} = -D\frac{1}{u_\tau}\frac{du_\tau}{dx} \qquad (2.6)$$

with $D = 1 + \kappa U_e{}^+$. Replacing in the integral von Kármán momentum equation $d\theta/dx = (U_e{}^+)^{-2}$ the definition of the momentum thickness θ and then using (2.5) and (2.6) it is found

$$\frac{1}{u_\tau}\frac{du_\tau}{dx} = \left\{ \int_0^\infty \left[\frac{U}{u_\tau} + y^+\frac{\partial U_i^+}{\partial y^+} - D\left(\eta\frac{\partial U_w^+}{\partial \eta} + \frac{1}{\kappa} \right) \right] \left[U_e{}^+ - 2\frac{U}{u_\tau} \right] dy \right\}^{-1} \qquad (2.7)$$

which finally allows the explicit determination of $\partial U/\partial x$, V and τ. The total shear stress is then modelled by $\tau/\rho = \nu_T(y)\partial U/\partial y$, where the total viscosity ν_T is the sum of the molecular and turbulent eddy viscosities; ν_T and its derivatives are explicitly computed inside the boundary layer, but in the potential region, say for $\eta > \eta_*$, where they respectively tend to ν and zero and are numerically undefined, since both τ and $\partial U/\partial y$ tend to zero, they are extrapolated. We have used $\eta_* = 0.25$, but the results of the extrapolation are not affected if η_* is changed, provided that it remains in the range ≈ 0.15–0.27.

2.2. *Linear perturbations and optimal growth*

Following the rationale of previous investigations of Reynolds & Tiederman (1967), Reynolds & Hussain (1972) and del Álamo & Jiménez (2006) we consider the linear temporal growth of perturbations $\boldsymbol{u} = (u, v, w)$, p to the turbulent mean flow, assumed parallel, $\boldsymbol{U} = (U(y), 0, 0)$ with eddy viscosity $\nu_T(y)$. These perturbations satisfy the

continuity equation $\nabla \cdot \boldsymbol{u} = 0$ and the linearized momentum equation

$$\frac{\partial \boldsymbol{u}}{\partial t} + U \frac{\partial \boldsymbol{u}}{\partial x} + (v\,U', 0, 0) = -\frac{1}{\rho}\nabla p + \nabla \cdot [\nu_T(y)(\nabla \boldsymbol{u} + \nabla \boldsymbol{u}^T)], \qquad (2.8)$$

where $(')$ stands for $\partial/\partial y$. Under the parallel flow assumption, perturbations of the form $\widehat{\boldsymbol{u}}(\alpha, y, \beta, t)\,e^{i(\alpha x + \beta z)}$ can be separately considered, where α and β are respectively the streamwise and spanwise wavenumbers. Standard manipulations (see, e.g. Schmid & Henningson 2001), generalized to include a variable viscosity (e.g. White 2006), allow to recast the linearized system into the generalized Orr–Sommerfeld and Squire equations for respectively the normal velocity $\widehat{v}(y)$ and vorticity $\widehat{\omega_y}(y)$:

$$\begin{bmatrix} D^2 - k^2 & 0 \\ 0 & 1 \end{bmatrix} \frac{\partial}{\partial t} \left\{ \begin{matrix} \widehat{v} \\ \widehat{\omega_y} \end{matrix} \right\} = \begin{bmatrix} \mathscr{L}_{\mathcal{OS}} & 0 \\ -i\beta U' & \mathscr{L}_{\mathcal{SQ}} \end{bmatrix} \left\{ \begin{matrix} \widehat{v} \\ \widehat{\omega_y} \end{matrix} \right\} \qquad (2.9)$$

with

$$\begin{aligned} \mathscr{L}_{\mathcal{OS}} = {} & -i\alpha[U(D^2 - k^2) - U''] \\ & + [\nu_T\,(D^2 - k^2)^2 + 2\nu_T'(D^3 - k^2 D) + \nu_T''(D^2 + k^2)], \qquad (2.10) \\ \mathscr{L}_{\mathcal{SQ}} = {} & -i\alpha U + [\nu_T(D^2 - k^2) + \nu_T' D], \qquad (2.11) \end{aligned}$$

where D, like $(')$, stands for $\partial/\partial y$ and $k^2 = \alpha^2 + \beta^2$. The perturbation velocity is zero at the wall, resulting in the usual boundary conditions $\widehat{v} = D\widehat{v} = \widehat{\omega}_y = 0$ at $y = 0$.

The optimal (temporal) energy growth G is defined in the usual way as the ratio of the kinetic energy associated with $\widehat{\boldsymbol{u}}$ at time t to the kinetic energy of the initial condition $\widehat{\boldsymbol{u}}_0$ optimized over all allowed $\widehat{\boldsymbol{u}}_0$: $G(\alpha, \beta, t) = \sup_{\widehat{\boldsymbol{u}}_0} \|\widehat{\boldsymbol{u}}\|^2 / \|\widehat{\boldsymbol{u}}_0\|^2$ with $\|\widehat{\boldsymbol{u}}\| = [\int_{\mathcal{V}} |\widehat{\boldsymbol{u}}|^2, d\mathcal{V}]^{1/2}$. The maximum optimal growth, defined as $G_{max}(\alpha, \beta) = \sup_t G(\alpha, \beta, t)$, is attained at the time t_{max}. The standard methods used to compute the maximum growth of laminar basic flows and described by, e.g. Schmid & Henningson (2001) are easily extended to the case of the variable viscosity $\nu_T(y)$. The numerical code is based on a spectral discretization of the operators $\mathscr{L}_{\mathcal{OS}}$ and $\mathscr{L}_{\mathcal{SQ}}$ obtained by using differentiation matrices (Weideman & Reddy 2000) based on Chebyshev polynomials on a grid of $Ny + 1$ collocation points in the interval $y \in [0, y_{max}]$. The perturbation velocity is required to vanish at the upper boundary y_{max}, but this artificial boundary condition does not affect the results provided that y_{max} is large enough. The code has been carefully validated in previous studies (e.g. Lauga & Cossu 2005), and its results have been carefully tested on a turbulent channel flow and the laminar boundary layer. The results discussed below have been obtained using 257 to 513 collocation points and y_{max} ranging from $0.4\,\Delta$ (almost twice the boundary layer thickness) for small wavelengths to $40\,\delta_*$ for the largest wavelengths. The convergence of the results has been checked by doubling the number of collocation points and/or the maximum domain extension to $80\,\delta_*$.

3. Results

3.1. *Basic flow*

The mean velocity profile given in (2.3) and the corresponding shear stress τ have been computed for a set of Reynolds number Re_{δ_*} and are reported in figure 1. For the considered profiles the boundary layer thickness, defined as the position at which $U = 0.99\,U_e$, is approximatively given by $\delta = 0.223\,\Delta$ for $Re_{\delta_*} \geqslant 10^4$. Monkewitz *et al.* (2007) have carefully validated with experimental data the mean profiles given by (2.3)
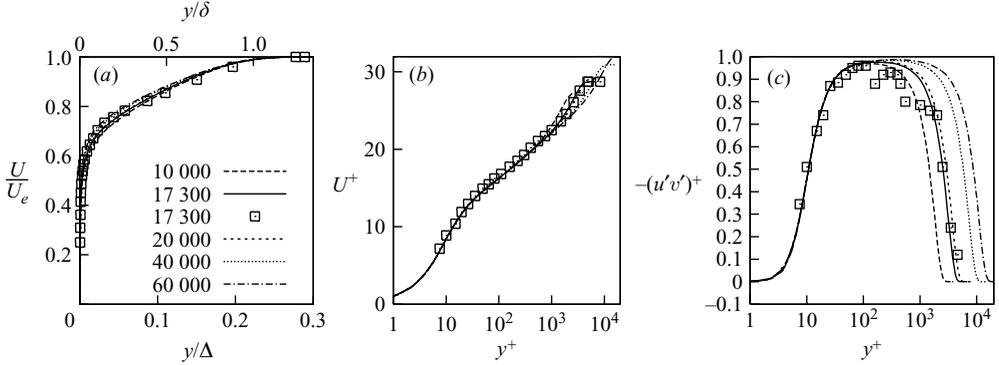
FIGURE 1. Turbulent mean flow profiles given by (2.3) plotted in (*a*) outer and (*b*) inner units. (*c*) Inner scaled Reynolds shear stress $-\langle u'v'\rangle/u_\tau^2 = (\tau/\rho - \nu U')/u_\tau^2$ plotted in inner scale y^+. The selected Reynolds numbers are $Re_{\delta_*} = 10^4, 1.73 \times 10^4, 2 \times 10^4, 4 \times 10^4, 6 \times 10^4$, and experimental data from de Graaff & Eaton (2000) at $Re_{\delta_*} = 1.73 \times 10^4$ are also reported for comparison as squares.
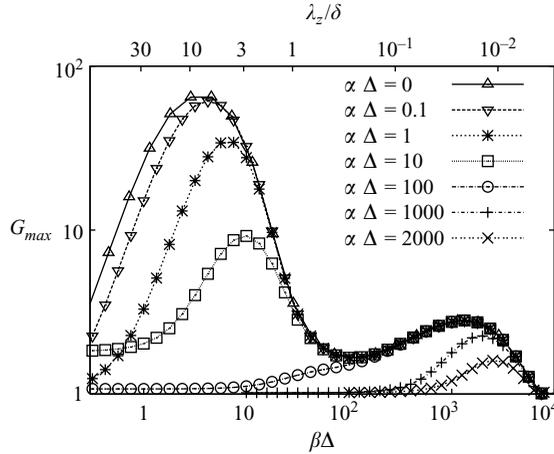

FIGURE 2. Dependence of the maximum growth G_{max} on the spanwise wavenumber $\beta\Delta$ obtained at $Re_{\delta_*} = 17\,300$ for selected streamwise wavenumbers ($\alpha\Delta = 0, 0.1, 1, \ldots$).

but not the corresponding shear stress that was not explicitly computed. We therefore compare the Reynolds shear stress, computed following the procedure described in §2.1, to the experimental data obtained by De Graaff & Eaton (2000) at $Re_{\delta_*} = 17\,300$ (corresponding to $Re_\theta = 13\,000$). As can be seen from figure 1(*c*), the theoretical and the experimental data agree reasonably well for both the velocity profiles and the Reynolds shear stress.

3.2. *Optimal perturbations and growth at fixed Reynolds number*

3.2.1. *Dependence of the optimal growth on the streamwise and spanwise wavenumbers*

We have initially computed the optimal perturbations and growth G_{max} of the mean flow obtained for $Re_{\delta_*} = 17\,300$ for a range of streamwise and spanwise wavenumbers extending from zero to $10^4/\Delta$. The results are reported in figure 2. As in the case of the canonical laminar shear flows and the turbulent channel flow, the largest growths are obtained for structures uniform in the streamwise direction ($\alpha = 0$), and significant
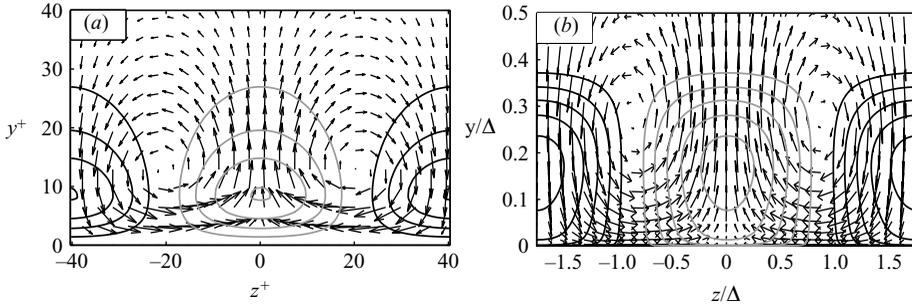
FIGURE 3. Cross-stream view of the v–w components of the optimal initial vortices (arrows) and the u component of the corresponding maximally amplified streak (contour lines) for $Re_{\delta_*} = 17\,300$, $\alpha = 0$. (a) The secondary peak optimal ($\beta\Delta = 1300$) is plotted in internal units, while (b) the primary peak optimal ($\beta\Delta = 3.65$) is plotted in external units. Black contours represent positive u, while grey contours represent negative u.

growths are observed only when $\alpha \leqslant \beta$, i.e. for structures elongated in the streamwise direction ($\lambda_x \geqslant \lambda_z$) . For streamwise uniform structures ($\alpha = 0$) the largest growth is attained by very large structures with $\beta\Delta = 3.7$, corresponding to $\lambda_z = 7.6\,\delta$. The optimal spanwise wavelength is strongly reduced when the perturbations have long but finite streamwise wavelengths λ_x. For instance an optimal $\lambda_z = 4.2\,\delta$ is found when $\lambda_x = 28\,\delta$ (corresponding to $\alpha\Delta = 1$).

A clearly distinct secondary peak can be identified at large spanwise wavenumbers ($\beta\Delta \sim 1300$ in external units) corresponding to structures with $\lambda_z^+ \sim 80$. The secondary peak becomes the only and the dominant one for perturbations of large streamwise wavenumber. The double peak structure, corresponding to two distinct outer and inner scalings, is very much like what is observed in the turbulent channel flow case by del Álamo & Jiménez (2006).

3.2.2. Streamwise uniform optimal perturbations

The $\alpha = 0$ optimals corresponding to the two peaks reported in figure 2 are displayed in figure 3. The optimal initial conditions consist of streamwise vortices (large v and w and very small u components) that induce, at the time of maximum growth, streamwise streaks (large u and small v and w components). The optimal streamwise vortices and streaks displayed in figure 3(a) and corresponding to the secondary peak at $\lambda_z^+ = 81.5$ are centred near $y^+ = 10$ like in the turbulent channel flow case of del Álamo & Jiménez (2006) in agreement with previous results on the sublayer streaks (e.g. del Álamo *et al.* 2004; Jiménez, del Álamo & Flores 2004). For the primary peak (figure 3b) the optimal initial vortices are centred above the edge of the boundary layer, and the corresponding optimal streaks have non-negligible amplitude inside boundary layer.

In figure 4 are reported the normalized amplitudes of the wall normal v component of the optimal initial condition ($t = 0$) and the streamwise u component of the optimal response ($t = t_{max}$) for different spanwise wavelengths λ_z. For all λ_z, the optimal initial conditions (vortices) are more concentrated in the wall normal direction and located farther from the wall than the corresponding optimal responses (streaks). When λ_z^+ is increased, starting from 100, the centre of the optimal vortices moves away from the wall (figure 4a) in an almost self-similar way. For $\lambda_z > 10\,\delta$ the primary peak optimal vortices (figure 4c) are localized outside the boundary layer, with a centre
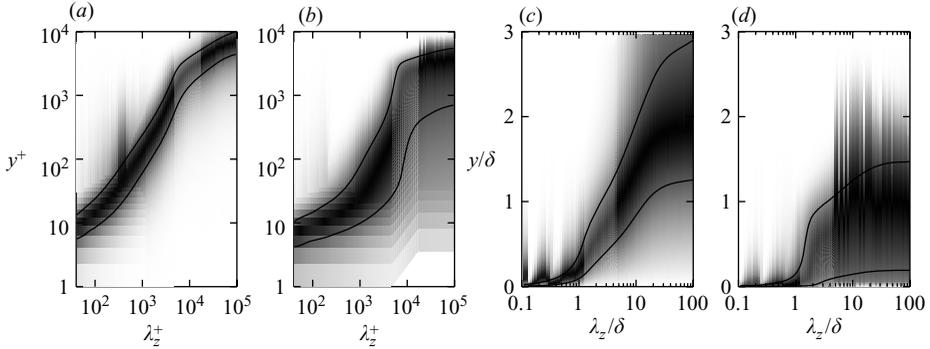
FIGURE 4. Normalized amplitude of (*a*), (*c*) the v component of the optimal initial vortices and (*b*), (*d*) the u component of the corresponding optimally amplified streaks for $Re_{\delta_*} = 17\,300$, $\alpha = 0$ respectively plotted in (*a*), (*b*) internal and (*c*), (*d*) external scales versus the wall normal coordinate for the considered spanwise wavelengths λ_z. To ease the comparison with experimental data, in external scaling the lengths have been scaled on $\delta = 0.223\,\Delta$. The greyscale intensity is proportional to the amplitude of the velocity component (the maximum amplitude being black); the two black lines correspond to 80 % of the maximum amplitude.
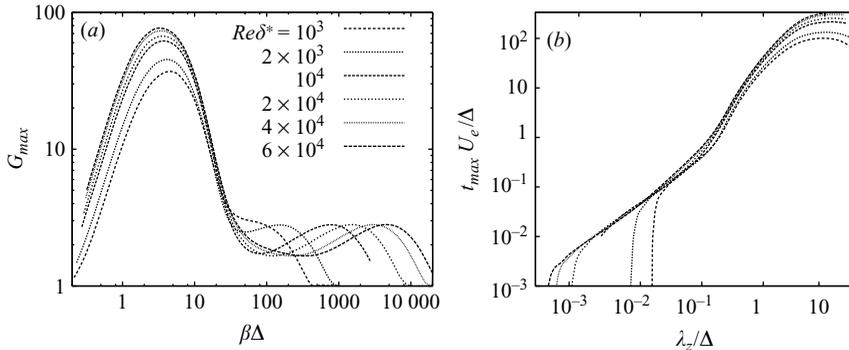

FIGURE 5. (*a*) Dependence on the spanwise wavenumber $\beta\Delta$ of the maximum growth G_{max} of streamwise uniform ($\alpha = 0$) perturbations for the selected Reynolds numbers Re_{δ_*}. (*b*) Times t_{max} at which the optimal growths reported in (*a*) are attained.

that remains near $y = 2\,\delta$ for $\lambda_z \geqslant 20$, while the optimally induced streaks (figure 4*d*) have the maximum near $y = \delta$ and extend well inside the boundary layer.

3.3. *Dependence on Reynolds number*

3.3.1. *Scaling of the maximum growth*

We have repeated the computations of the optimals for an additional set of low (10^3, 2×10^3) and relatively large (10^4, 2×10^4, 4×10^4 and 6×10^4) Reynolds numbers Re_{δ_*} considering only streamwise uniform ($\alpha = 0$) perturbations, which are the most amplified. As expected, the inner and the outer peaks are separated only at sufficiently large Reynolds number (indicatively for $Re_{\delta_*} > 1500$) as can be seen from figure 5(*a*), where the curves $G_{max}(\alpha = 0, \beta)$ are reported for the considered set of Re_{δ_*}. The maximum growth, corresponding to the primary peak, increases with Re_{δ_*} and is attained for essentially the same range of spanwise scales in external units, while the secondary peak growth is essentially independent of Re_{δ_*} and is shifted to larger β (smaller λ_z) when Re_{δ_*} is increased. The time t_{max} at which the optimals are reached
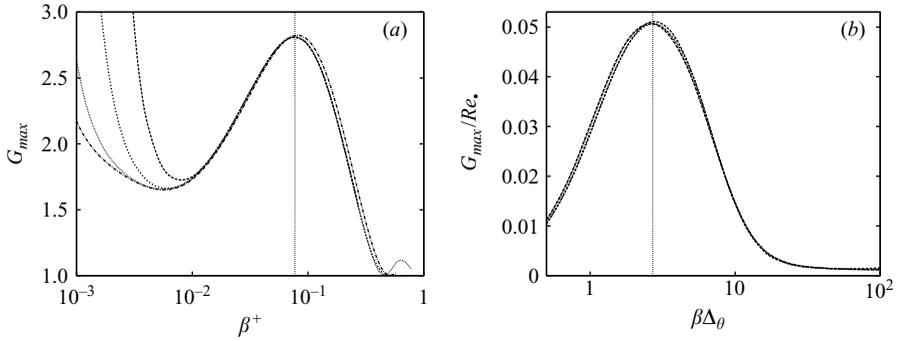
FIGURE 6. Large Reynolds number ($Re_{\delta_*} = 10^4, \ldots, 6 \times 10^4$) optimal growth data already reported in figure 5 but rescaled in (*a*) inner units and zoomed on the secondary peak represented by the vertical line at $\beta^+ = 0.077$ ($\lambda^+ = 81.6$) and (*b*) outer units with the modified Rotta–Clauser length Δ_θ and the effective Reynolds number $Re_\bullet$ and zoomed on the primary peak represented by the vertical line at $\beta\Delta_\theta = 2.7$. The legends in (*a*) and (*b*) are the same as the ones used in figure 5, but in (*b*) the four curves are almost indistinguishable.

is approximately proportional to λ_z (figure 5*b*), as already noticed in the case of the turbulent channel flow by del Álamo & Jiménez (2006). An overshoot in t_{max} however appears when $\lambda_z > 0.1\Delta$.

The large Reynolds number ($Re_{\delta_*} \geqslant 10^4$) optimal growth data reported in figure 5 are redisplayed in inner units in figure 6(*a*) and zoomed on the lower peak. In inner units the data corresponding to all the considered Reynolds numbers collapse on a single curve with a maximum amplification of $G_{max}^{(inn)} = 2.8$ obtained for $\beta_{max}^{+(inn)} = 0.077 \pm 0.001$, corresponding to an optimal $\lambda_z^+ = 81.5 \pm 1$. As already remarked, the maximum growth in the secondary peak does not seem to depend on the Reynolds number when Re_{δ_*} is sufficiently large.

The primary, dominant peak scales in outer units. In the channel flow case the unique outer length scale is the channel half-width h. For a boundary layer, different choices, like δ_*, θ and Δ, are available, but they are not equivalent when the boundary layer mean profiles are not self-similar, like in the present case. The Rotta–Clauser length Δ is the more natural length to use, since it is the external scale used to build the mean velocity profile. However, as seen from figure 5, the spanwise wavenumber of maximum amplification does not scale on this length, which is probably due to the fact that the shape factor $H = \delta_*/\theta$ of the mean flow depends on the Reynolds number. For laminar boundary layers with pressure gradient, where the shape factor depends on the pressure gradient, Corbett & Bottaro (2000) found that the most relevant length is the momentum thickness θ. In our case we therefore consider a modified Rotta-Clauser length, no longer based on the displacement thickness but on the momentum thickness: $\Delta_\theta = \theta U_e/u_\tau$. This new characteristic length is related to the Rotta–Clauser length by $\Delta_\theta = \Delta/H$. The most amplified wavenumber is seen to fairly scale on Δ_θ for sufficiently large Re_{δ_*} with $\beta_{max}^{(out)}\Delta_\theta = 2.7 \pm 0.1$. In the case of laminar flows the maximum energy growth scales on the square of the Reynolds number based on the outer length scale and velocity and the molecular viscosity. In the present turbulent mean flow case, for the outer structures it is natural to use the external velocity U_e and the relevant length scale Δ_θ; furthermore, the choice of the maximum total viscosity $\nu_{Tmax} = \sup_y \nu_T(y)$ leads to the definition of an 'effective' Reynolds number $Re_\bullet = U_e\Delta_\theta/\nu_{Tmax}$. For the considered mean flow profiles $Re_\bullet$ ranges approximately from 1200 to 1500 for $Re_{\delta_*} \in [10\,000, 60\,000]$. For $Re_\bullet \geqslant 1000$ the maximum growth data are seen to very well collapse on a single curve when
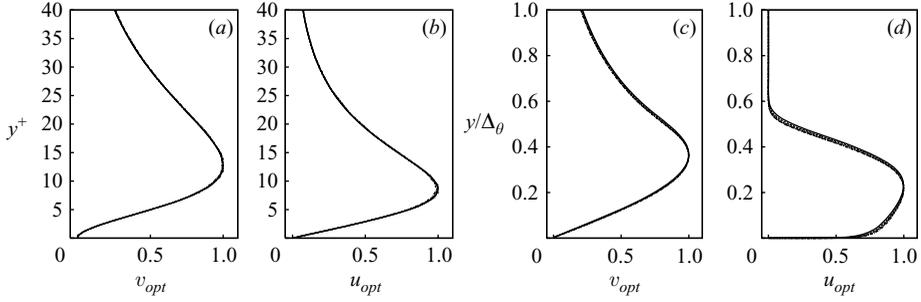
FIGURE 7. (a and c): Normalized amplitude of the v component of the optimal initial ($t=0$) vortices (b and d): the u component of the corresponding optimally amplified ($t=t_{max}$) streaks respectively corresponding to the inner (a, b) and outer (c, d) peaks plotted versus the wall normal coordinate respectively scaled in inner and outer scales. The four curves corresponding to $Re_{\delta_*} = 10\,000, 20\,000, 40\,000$ and $60\,000$ are almost undistinguishable. The legends are the same as figure 5.

rescaled on $Re_\bullet$ and $\beta\Delta_\theta$, as shown in figure 6(b). In particular, it is found that $G_{max}^{(out)} = (0.0508 \pm 0.0004) Re_\bullet$. It is important to stress that in this turbulent case the the dependence of G_{max} on the Reynolds number is linear, while it is quadratic in the laminar case. Attempts to rescale the data on other Reynolds numbers based on the molecular kinematic viscosity ν and/or non-Rotta–Clauser length scales, such as δ_* and θ produced less correlated (more scattered) results.

3.3.2. Scaling of the optimal perturbations

In figure 7 the wall normal velocity component v of the optimal initial vortices and the streamwise velocity component u of the optimally induced streaks corresponding to the primary and secondary peaks are plotted versus respectively the wall normal inner (y^+) and outer (y/Δ_θ) coordinates. When rescaled in proper units the optimal perturbations are seen to assume a shape independent of the Reynolds number. For the inner peak, the maximum of the optimal initial v, giving the distance from the wall of the centre of the optimal initial counter-rotating vortices, is situated approximately at $y^+ = 13$, while the maximum of the optimal final u is situated near $y^+ = 8.5$. Considering the outer peak, the maximum of the optimal initial v is situated approximatively at $y = 0.36\,\Delta_\theta$, just above the edge of the boundary layer. The maximum of optimal outer streak is situated at $y = 0.22\,\Delta_\theta$, inside the boundary layer, but as already remarked, these streaks have non-negligible amplitude in almost the entire boundary layer.

The u component of the optimal outer peak streaks already reported in figure 7(d) is replotted in inner variables in figure 8 for the same set or Re_{δ_*} expressing u_{opt} in friction velocity units by using the factor $U_e^+(Re_{\delta_*})/U_e^+(10^4)$ in which $Re_{\delta_*} = 10^4$ is taken as the reference case. The $u^{+(out)}_{opt}(y^+)$ curves collapse on a single curve in the log and near wall regions in which they are proportional to the mean flow velocity profile. In figure 8, the $Re_{\delta_*} = 10^4$ mean velocity profile rescaled to have unit amplitude at the position of the maximum of the corresponding streak (where the streak amplitude is also normalized to one) is also reported for comparison. This particular scaling of the optimal streaks allow them to have very large amplitude inside the near wall region, just like the mean flow: at $y^+ = 20$ they still have half of their maximum amplitude.
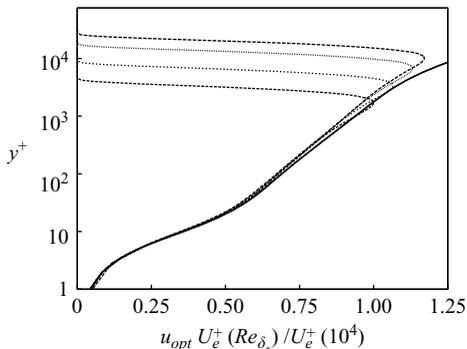
FIGURE 8. Normalized u component of the optimally amplified ($t = t_{max}$) streaks of the primary (outer) redisplayed in wall units and normalized on the $Re_{\delta_*} = 10^4$ reference case. Same data and legends as in figure 7(d). The mean flow profile corresponding to $Re_{\delta_*} = 10^4$ and normalized to unity at the position of the maximum of the corresponding optimal streaks is also reported for comparison as a solid thick line.

4. Summary and discussion

4.1. *Summary of the main results*

The optimal linear mean perturbations and growth have been computed for a zero pressure gradient turbulent boundary layer modelled with the two-scale composite expansion of Monkewitz *et al.* (2007) which has been previously validated with large Reynolds number experimental data. The turbulent eddy viscosity associated with the selected basic flows is included in the linearized operator. The main results found in this investigation are as follows:

(a) All the considered turbulent boundary layers are linearly stable but sustain transient energy growths.

(b) Only disturbances with streamwise wavelength λ_x larger than the spanwise wavelength λ_z are noticeably transiently amplified, the most amplified one always being streamwise uniform.

(c) For sufficiently large Reynolds numbers two distinct peaks of the optimal growth exist for streamwise uniform perturbations: a primary peak scaling in outer variables and a secondary peak scaling in inner variables.

(d) The energy growth associated with the secondary peak is small ($G_{max} = 2.8$), independent of the Reynolds number and attained by vortices and streaks with a spanwise wavelength $\lambda_z^+ = 81.6$.

(e) The energy growth associated with the primary peak is larger than that of the inner peak ($G_{max} > 60$ when $Re_{\delta_*} > 10^4$) and scales on a Reynolds number $Re_\bullet = U_e \Delta_\theta / \nu_{T\,max}$ based on the external velocity, the maximum eddy viscosity and a modified Rotta–Clauser length based on the momentum thickness $\Delta_\theta = \theta U_e / u_\tau$. The scaling is linear and not quadratic like in the laminar case.

(f) The primary peak is realized by optimal perturbations that have a very large spanwise wavelength $\lambda_z \sim 8\,\delta$. The optimal initial vortices are centred near the edge of the boundary layer, and the corresponding streaks extend inside all the boundary layer and have non-negligible amplitudes inside all the viscous layer. The optimal velocity profiles scale on Δ_θ, but in the viscous layer the amplitude of the optimal streaks is proportional to the local mean velocity and scales in inner units.

(g) Intermediate optimal vortices and streaks, with spanwise wavelength between the two peaks, have a wall normal extension approximately proportional to their spanwise wavelength.

4.2. *Limitations of the results due to the parallel flow assumption*

To compute the linear optimals a parallel flow assumption has been made for the basic mean flow. Since the boundary layer thickness doubles in about $50-100\delta$, corresponding to $10-20\Delta$, depending on the Reynolds number, a standard Wentzel–Kramers–Brillouin–Jeffreys (WKBJ) approach would formally be limited to perturbations with $\lambda_x < 50$–100δ, corresponding to $\alpha\Delta > 0.3$–0.6. All the presented results not respecting this limitation, and in particular those obtained for the optimal streamwise uniform structures ($\alpha = 0$), are therefore subject to caution. The same issue has already been addressed in the case of the optimal perturbations of the laminar boundary layer (the Blasius profile). Butler & Farrell (1992), under the parallel flow assumption, found the optimals $\alpha\delta_* = 0$, $\beta\delta_* = 0.65$ and a maximum growth $G_{max} = 1.5\,10^{-3}Re_{\delta_*}^2$. Using the fully non-parallel approach and forcing the optimal vortices at the leading edge of the flat plate (where $\delta_* = 0$), Andersson, Berggren & Henningson (1999) and Luchini (2000) found $\alpha\delta_* = 0$, $\beta\delta_* = 0.77$ and $G_{max} = 0.784\,10^{-3}Re_{\delta_*}^2$. In the laminar case the parallel flow analysis is therefore able to predict the qualitative features of the optimals like their streamwise uniform nature ($\alpha = 0$), the scaling of G_{max} with Re_{δ_*} and the shape of the optimal perturbations. The parallel flow predictions however overestimate $\beta\delta_*$ by 18 % and $G_{max}/Re_{\delta_*}^2$ by almost a factor 2. However, in the cited non-parallel analyses the optimal vortices are forced at leading edge of the flat plate ($x = 0$, where $\delta_* = 0$) which is the worst case to compare with parallel flows approximations, and the results are made dimensionless with the δ_* corresponding to the final position at which the maximum amplitude of the streaks is observed, which again is the worst choice for a comparison. In passive control applications (e.g. Fransson *et al.* 2004, 2006) vortices are forced downstream at an already large Re_{δ_*}, and in this case the parallel flow theories should give even more accurate predictions. Of course a fully non-parallel analysis could also be desirable for the turbulent boundary layer case. However, if the optimal vortices are to be forced at the leading edge, such an analysis would require to take into account the laminar and the transitional regions, leading to an even more complex study. Furthermore, the relevance of non-parallel, very accurate predictions could be questioned given the very crude assumptions made for the turbulence dynamics (modelled with ν_T).

4.3. *Scaling of the inner and outer peaks*

The existence of two different peaks for the optimal growth and their respective scaling in inner and outer units confirms and extends the results found in the turbulent channel flow by del Álamo & Jiménez (2006). This 'bimodal' distribution with an outer-scaling peak whose amplitude increases with the Reynolds number and the distance from the wall is furthermore compatible with the experimental results of Hites (1997) and Österlund *et al.* (2000) among others. The fact that the maximum growth corresponding to the inner peak does not depend on the Reynolds number has already been explained by del Álamo & Jiménez (2006) using two facts: one, the time of maximum growth scales linearly with the spanwise wavelength with $t_{max}^+ \sim 0.1\lambda_z^+$ (which we also found in our results); two, in the inner region the eddy viscosity is $\nu_T \sim u_\tau\lambda_z$. The effective Reynolds number $Re_T = \lambda_z^2/(\nu_T t_{max})$ associated with the maximum transient growth is readily seen to be constant with $Re_T \sim 10$, which also explains the low values of G_{max} at the inner peak. The independence of G_{max} from the Reynolds number breaks down for the outer peak because for

the outer optimals, extending outside the log layer; t^+_{max} is no more exactly proportional to λ^+; and the assumption $\nu_T \sim u_\tau \lambda_z$ does not hold any more.

4.4. *Structures associated with the peak scaling in inner units*

The spanwise wavelength corresponding to the secondary peak, $\lambda^+_z = 81.6$, is lower than the commonly accepted value of 100^+ for the spacing of the buffer layer streaks reported by, for instance Kline *et al.* (1967) and Smith & Metzler (1983). However, as discussed by Smith & Metzler (1983), $\lambda^+_z = 100$ is the 'mean' value for the streak spacing, while the 'most probable' value is 20 % lower, i.e. nearly $\lambda^+_z = 80$, which is in fairly good agreement with our results. The most amplified $\lambda^+_z = 80$ could therefore be related to the most probable streak spanwise wavelength, while the mean is shifted towards larger λ^+_z because they are more amplified than the smaller ones as it is apparent from figure 6. The structure and scaling of the intermediate (in between peaks) optimals is also in accordance with the experimental observations of Tomkins & Adrian (2003) and the channel flow results of del Álamo & Jiménez (2006).

4.5. *Robustness of the outer peak to the choice of the eddy viscosity*

In the laminar and turbulent channel flows the outer optimal is attained with perturbations with similar spanwise scales: Butler & Farrell (1992) found $\lambda_z \sim 3\,h$ for the laminar case just as Butler & Farrell (1993) and del Álamo & Jiménez (2006) did for the turbulent case. (However Pujals *et al.* (in press) found a slightly larger $\lambda_z \sim 4\,h$ for the turbulent channel flow.) In the present turbulent boundary layer case the optimal spanwise scale $\lambda_z \sim 8\,\delta$ is much larger than the optimal laminar value $\lambda_z \sim 3.3\,\delta$ found by Butler & Farrell (1992). This difference persists even when λ_z is scaled on the displacement or the momentum thickness. To understand if this large optimal λ_z is mainly selected by the mean flow profile, which is a robust characteristic of the boundary layer, or the eddy viscosity, which could be more dependent on the assumptions made in its derivation, we have recomputed the optimal growth, using a constant viscosity for $Re_{\delta_*} = 17\,300$. When the constant kinematic viscosity is assumed equal to the molecular ν, i.e. using the same approach of Butler & Farrell (1993), we similarly find a large peak ($G_{max} = 7467$), but this peak is obtained for the large $\lambda_z \sim 11\,\delta$. When the artificially constant viscosity is assumed equal to $\nu_{T\,max}$, the maximum growth is reduced ($G_{max} = 5.67$) and obtained with the optimal $\lambda_z \sim 4\,\delta$. In both cases an optimal λ_z larger than the laminar value is found, the optimal $\lambda_z \sim 8\,\delta$ obtained with the 'correct' eddy viscosity $\nu_T(y)$ being situated in between the two extrema. An optimal λ_z larger than the laminar optimal seems therefore to be a robust feature of the turbulent boundary layer not very sensitive to the shape of the eddy viscosity.

4.6. *Structures associated with the peak scaling in outer units*

As it is well known large-scale structures, observed in the outer layer (e.g. Kovasznay, Kibens & Blackwelder 1970), can extend deep inside the viscous layer (e.g. Morrison, Bullock & Kronauer 1971; Townsend 1976; Hoyas & Jiménez 2006; Jiménez 2007 and the references therein). This is also the case for the optimal streaks associated with the outer peak that strongly protrude with large amplitudes inside the viscous layer in which they furthermore have amplitudes proportional to the mean velocity. One can then expect to find a signature of these optimal streaks in experimental measures of turbulent boundary layers. However very large–scale structures with $\lambda_z \approx 4 - 8\delta$ have not yet been observed in experiments or numerical simulations. There are different possible reasons of this lack of observation:

(*a*) The parallel flow assumption. This assumption has a tendency to overestimate the spanwise wavelength, but in the laminar flow case this error was of the order of 20 % and would be less if the optimal perturbations are not forced at the leading edge but further downstream or if appropriate average δ_* are taken for comparison of parallel and non parallel results.

(*b*) The finite streamwise size of the observed streaks. In typical experiments, such as those of Tomkins & Adrian (2003), the structures observed have streamwise lengths of the order of $\lambda_x \approx 2\text{--}2.5\delta$ corresponding to $\alpha\Delta \approx 14\text{--}11$. For these perturbations the optimal perturbations have shorter spanwise wavelengths $\lambda_z \approx 1\text{--}3\delta$, which is compatible with the observations.

(*c*) The size of the data acquisition window. The largest field of view in the experiments of Tomkins & Adrian (2003) is limited to 2.5δ in the streamwise direction and 3.15δ in the spanwise direction, and therefore the structures corresponding to the outer peaks with $\alpha\Delta < 1$ ($\lambda_x > 28\delta$) that have $4\delta < \lambda_z < 8\delta$ could not be detected. In the more recent experiments of Hutchins & Marusic (2007), structures with $\lambda_x < 20\delta$ are measured, but the spanwise field of view is limited to 2δ, precluding again the observation of larger structures.

(*d*) The selection of the spanwise wavelength by nonlinear effects. The transient growth of vortices into streaks is only a part of the more complicated processes like the one leading to self-sustained cycles. It could be that very large–scale structures are not selected for a self-sustained process nor passively forced by other self-sustained processes. In this case these structures would have to be artificially forced to be detected, like it has been done by Kitoh & Umeki (2008) in the turbulent Couette flow.

Even if the question of the relevance of the optimal large-scale structures to real-world, unforced turbulent boundary layers is still open, these structures may have an important role in active or passive control applications.

Appendix A. Explicit expression of the mean velocity profile

We report the explicit expressions of the mean velocity profile expressions proposed by Monkewitz *et al.* (2007):

$$U_w^+(\eta) = \left[\frac{1}{\kappa}E_1(\eta) + w_0\right]\frac{1}{2}\left[1 - \tanh\left(\frac{w_{-1}}{\eta} + w_2\eta^2 + w_8\eta^8\right)\right] \tag{A 1}$$

with $w_0 = 0.6332$, $w_{-1} = -0.096$, $w_2 = 28.5$ and $w_8 = 33\,000$,

$$U_{log}^+(y^+) = \frac{1}{\kappa}\ln(y^+) + B \tag{A 2}$$

$$U_e^+(Re_{\delta_*}) = \frac{1}{\kappa}\ln(Re_{\delta_*}) + C, \tag{A 3}$$

where $\kappa = 0.384$, $B = 4.17$, $C = 3.3$;

$$\begin{aligned}
U_i^+(y^+) = {} & 0.68285472\ln(y^{+2} + 4.7673096y^+ + 9545.9963), \\
& + 1.2408249\arctan(0.010238083y^+ + 0.024404056), \\
& + 1.2384572\ln(y^+ + 95.232690) - 11.930683, \\
& - 0.50435126\ln(y^{+2} - 7.8796955y^+ + 78.389178), \\
& + 4.7413546\arctan(0.12612158y^+ - 0.49689982), \\
& - 2.7768771\ln(y^{+2} + 16.209175y^+ + 933.16587), \\
& + 0.37625729\arctan(0.033952353y^+ + 0.27516982), \\
& + 6.5624567\ln(y^+ + 13.670520) + 6.1128254.
\end{aligned} \tag{A 4}$$

REFERENCES

DEL ÁLAMO, J. C. & JIMÉNEZ, J. 2006 Linear energy amplification in turbulent channels. *J. Fluid Mech.* **559**, 205–213.

DEL ÁLAMO, J. C., JIMÉNEZ, J., ZANDONADE, P. & MOSER, R. D. 2004 Scaling of the energy spectra of turbulent channels. *J. Fluid Mech.* **500**, 135–144.

ANDERSSON, P., BERGGREN, M. & HENNINGSON, D. 1999 Optimal disturbances and bypass transition in boundary layers. *Phys. Fluids* **11** (1), 134–150.

BOTTARO, A., SOUIED, H. & GALLETTI, B. 2006 Formation of secondary vortices in a turbulent square-duct flow. *AIAA J.* **44**, 803–811.

BUTLER, K. M. & FARRELL, B. F. 1992 Three-dimensional optimal perturbations in viscous shear flow. *Phys. Fluids* A **4**, 1637–1650.

BUTLER, K. M. & FARRELL, B. F. 1993 Optimal perturbations and streak spacing in wall-bounded turbulent shear flow. *Phys. Fluids* **5**, 774–777.

CESS, R. D. 1958 A survey of the literature on heat transfer in turbulent tube flow. *Res. Rep.* 8–0529–R24. Westinghouse.

CORBETT, P. & BOTTARO, A. 2000 Optimal perturbations for boundary layers subject to streamwise pressure gradient. *Phys. Fluids* **12**, 120–130.

COSSU, C. & BRANDT, L. 2002 Stabilization of Tollmien–Schlichting waves by finite amplitude optimal streaks in the Blasius boundary layer. *Phys. Fluids* **14**, L57–L60.

DE GRAAFF, D. B. & EATON, J. K. 2000 Reynolds-number scaling of the flat-plate turbulent boundary layer. *J. Fluid Mech.* **422**, 319–346.

ELLINGSEN, T. & PALM, E. 1975 Stability of linear flow. *Phys. Fluids* **18**, 487.

FARRELL, B. F. & IOANNOU, P. J. 1993 Optimal excitation of three-dimensional perturbations in viscous constant shear flow. *Phys. Fluids* **5**, 1390–1400.

FARRELL, B. F. & IOANNOU, P. J. 1996 Generalized stability theory. Part I: autonomous operators. Part II: nonautonomous operators. *J. Atmos. Sci.* **53**, 2025–2053.

FARRELL, B. F. & IOANNOU, P. J. 1998 Perturbation structure and spectra in turbulent channel flow. *Theoret. Comput. Fluid Dyn.* **11**, 237–250.

FRANSSON, J., BRANDT, L., TALAMELLI, A. & COSSU, C. 2004 Experimental and theoretical investigation of the non-modal growth of steady streaks in a flat plate boundary layer. *Phys. Fluids* **16**, 3627–3638.

FRANSSON, J., BRANDT, L., TALAMELLI, A. & COSSU, C. 2005 Experimental study of the stabilisation of Tollmien–Schlichting waves by finite amplitude streaks. *Phys. Fluids* **17**, 054110.

FRANSSON, J., TALAMELLI, A., BRANDT, L. & COSSU, C. 2006 Delaying transition to turbulence by a passive mechanism. *Phys. Rev. Lett.* **96**, 064501.

GUSTAVSSON, L. H. 1991 Energy growth of three-dimensional disturbances in plane Poiseuille flow. *J. Fluid Mech.* **224**, 241–260.

HAMILTON, J. M., KIM, J. & WALEFFE, F. 1995 Regeneration mechanisms of near-wall turbulence structures. *J. Fluid Mech* **287**, 317–348.

HITES, M. H. 1997 Scaling of high-Reynolds number turbulent boundary layers in the national diagnostic facility. PhD thesis, Illinois Institute of Technology, Chicago, IL, USA.

HOYAS, S. & JIMÉNEZ, J. 2006 Scaling of the velocity fluctuations in turbulent channels up to $re_\tau = 2003$. *Phys. Fluids* **18**, 011702.

HUTCHINS, N. & MARUSIC, I. 2007 Evidence of very long meandering features in the logarithmic region of turbulent boundary layers. *J. Fluid Mech.* **579**, 1–28.

JIMÉNEZ, J. 2007 Recent developments on wall-bounded turbulence. *Rev. R. Acad. Cien.* A **101**, 187–203.

JIMÉNEZ, J., DEL ÁLAMO, J. C. & FLORES, O. 2004 The large-scale dynamics of near-wall turbulence. *J. Fluid Mech.* **505**, 179–199.

JIMÉNEZ, J. & MOIN, P. 1991 The minimal flow unit in near-wall turbulence. *J. Fluid Mech.* **225**, 213–240.

KITOH, O. & UMEKI, M. 2008 Experimental study on large-scale streak structure in the core region of turbulent plane Couette flow. *Phys. Fluids* **20**, 025107.

KLINE, S. J., REYNOLDS, W. C., SCHRAUB, F. A. & RUNSTADLER, P. W. 1967 The structure of turbulent boundary layers. *J. Fluid Mech.* **30**, 741–773.

Kovasznay, L. S. G., Kibens, V. & Blackwelder, R. F. 1970 Large-scale motion in the intermittent region of a turbulent boundary layer. *J. Fluid Mech.* **41**, 283–325.

Kreiss, G., Lundbladh, A. & Henningson, D. S. 1994 Bounds for threshold amplitudes in subcritical shear flows. *J. Fluid Mech.* **270**, 175–198.

Landahl, M. T. 1980 A note on an algebraic instability of inviscid parallel shear flows. *J. Fluid Mech.* **98**, 243.

Lauga, E. & Cossu, C. 2005 A note on the stability of slip channel flows. *Phys. Fluids* **17**, 088106.

Luchini, P. 2000 Reynolds-number independent instability of the boundary layer over a flat surface. Part 2. Optimal perturbations. *J. Fluid Mech.* **404**, 289–309.

Malkus, W. V. R. 1956 Outline of a theory of turbulent shear flow. *J. Fluid Mech.* **1**, 521–539.

Moffatt, H. K. 1967 The interaction of turbulence with strong wind shear. In *Proc. URSI-IUGG Coloq. on Atoms. Turbulence and Radio Wave Propagation* (ed. A. M. Yaglom & V. I. Tatarsky), pp. 139–154. Nauka.

Monkewitz, P. A., Chauhan, K. A. & Nagib, H. M. 2007 Self-consistent high-Reynolds-number asymptotics for zero-pressure-gradient turbulent boundary layers. *Phys. Fluids* **19**, 115101.

Morrison, W. R. B., Bullock, K. J. & Kronauer, R. E. 1971 Experimental evidence of waves in the sublayer. *J. Fluid Mech.* **47**, 639–656.

Nagib, H. M., Christophorou, C. & Monkewitz, P. A. 2004 High Reynolds number turbulent boundary layers subjected to various pressure-gradient conditions. In *IUTAM Symposium on One Hundered Years of Boundary Layer Research* (ed. G. Meier & K. Sreenivasan), pp. 383–394. Springer.

Österlund, J. M. 1999 Experimental studies of zero-pressure gradient tubulent boundary layer flows. PhD thesis, Royal Insitute of Technology (KTH), Stockholm, Sweden.

Österlund, J. M., Johansson, A. V., Nagib, H. M. & Hites, M. H. 2000. A note on the overlap region in turbulent boundary layers. *Phys. Fluids* **12**, 1.

Pujals, G., García-Villalba, M., Cossu, C. & Depardon, S. In press. A note on optimal transient growth in turbulent channel flows. *Phys. Fluids*.

Reddy, S. C., Schmid, P. J., Baggett, J. S. & Henningson, D. S. 1998 On the stability of streamwise streaks and transition thresholds in plane channel flows. *J. Fluid Mech.* **365**, 269–303.

Reynolds, W. C. & Hussain, A. K. M. F. 1972 The mechanics of an organized wave in turbulent shear flow. Part 3. Theoretical models and comparisons with experiments. *J. Fluid Mech.* **54** (02), 263–288.

Reynolds, W. C. & Tiederman, W. G. 1967 Stability of turbulent channel flow, with application to Malkus's theory. *J. Fluid Mech.* **27** (02), 253–272.

Schlichting, H. 1979 *Boundary-Layer Theory*. Mc Graw-Hill.

Schmid, P. J. & Henningson, D. S. 2001 *Stability and Transition in Shear Flows*. Springer.

Smith, J. R. & Metzler, S. P. 1983 The characteristics of low-speed streaks in the near-wall region of a turbulent boundary layer. *J. Fluid Mech.* **129**, 27–54.

Tomkins, C. D. & Adrian, R. J. 2003 Spanwise structure and scale growth in turbulent boundary layers. *J. Fluid Mech.* **490**, 37–74.

Townsend, A. 1976 *The Structure of Turbulent Shear Flow*. Cambridge U. Press, second edition.

Trefethen, L. N., Trefethen, A. E., Reddy, S. C. & Driscoll, T. A. 1993 A new direction in hydrodynamic stability: beyond eigenvalues. *Science* **261**, 578–584.

Waleffe, F. 1995 Hydrodynamic stability and turbulence: Beyond transients to a self-sustaining process. *Stud. Appl. Math.* **95**, 319–343.

Weideman, J. A. C. & Reddy, S. C. 2000 A MATLAB differentiation matrix suite. *ACM Trans. Math. Soft.* **26** (4), 465–519.

White, F. M. 2006 *Viscous Fluid Flows*, 3rd edition. Mc Graw-Hill.